Biomaterials 32 (2011) 4877–4884

Contents lists available at ScienceDirect

Biomaterials

journal homepage: www.elsevier.com/locate/biomaterials

Polyhedral silver mesocages for single particle surface-enhanced Raman scattering-based biosensor

Jixiang Fang [a,c,*], Siyun Liu [b], Zhiyuan Li [b]

[a] School of Science, 'Xi'an Jiaotong University, Shann Xi 710049, People's Republic of China
[b] Institute of Physics, Chinese Academy of Sciences, Beijing 100090, People's Republic of China
[c] Karlsruhe Institut für Technologie (KIT), Institut für Nanotechnologie, Karlsruhe 76021, Germany

ARTICLE INFO

Article history:
Received 2 March 2011
Accepted 12 March 2011
Available online 13 April 2011

Keywords:
Single particle SERS
Polyhedral Ag mesocages
Biosensor
Ag_2O template

ABSTRACT

Surface-enhanced Raman scattering-based signal detection and molecular identification faces the lack of reproducibility and reliability thus hampers its practical applications. Here, we demonstrate a facile particle mediated aggregation protocol to synthesize highly roughened mesosuperstructure - silver polyhedral mesocages. The individual silver octahedral mesocage, owing to highly-roughed surface topography, anisotropic growth as well as intraparticle effect, creates homogenously distributed multiple effective hot spots on the surface of single mesoparticle, hereby exhibits a high reproducibility and an unusual SERS enhancement, i.e., $\sim 10^8$–10^9 magnitude. As such, the current protocol opens avenues for the fabrication of structurally reproducible mesosuperstructure-based SERS sensors.

1. Introduction

Surface-enhanced Raman scattering (SERS) - based signal detection and molecular identification have been intensively investigated in the last decade [1–5]. The enormous potential applications of extremely sensitive SERS have attracted considerable interests in the nanomaterials, biotechnologies and etc [6–8]. Currently, the SERS-based molecule detection faces a problem in the lack of reproducibility and reliability [9,10]. "Hot spots" (or called hot sites) are the regions where the surface plasmons highly localize, giving rise to very large field enhancements, $\sim 10^{10}$–10^{11}, that SERS detection at or near single molecule sensitivity [11]. Recent investigations, for example, using the technique of tip enhanced Raman scattering (TERS) [12] and the electron energy-loss spectroscopy (EELS) [13] have proven that hot spots arise at nanogaps between two closely-spaced metallic objects or a sharp structure or a combination of both, and play an important part in extremely sensitive SERS. On the other hand, only a small proportion of colloid aggregates (hot particles) seem to contribute to main SERS signals, e.g., in ref [14]: the hottest SERS-active sites (local enhancement factor is $>10^9$) accounted for only 63 sites in 1,000,000 of the total sites, but contributed 24% of the overall SERS intensity. In these regards, assembling SERS-active nanoparticles into well-defined and reproducible hot SERS nanostructures and subsequent detection of Raman signals from individual SERS-active nanostructures would be very crucial [15]. Unfortunately, although the detailed geometry and performance of such hot spots are well understood [12,13], their controlled fabrication is not achieved, thus the less reproducibility and repeatability of the SERS substrate hinder its practical applications.

Here, with the aim of creating abundant amount of the effective hot spots, and simultaneously keeping the high reliability and reproducibility, a particle mediated aggregation strategy is suggested to synthesize mesosuperstructure (or mesoassembly)-polyhedral mesocages. Noble metal nanocages (e.g., Au, Ag) represent a class of nanostructures with high surface areas, low densities, hollow interiors and porous walls. They can display a strong capability of tailoring the surface plasmon resonance (SPR) properties (apparent red shift relative to solid Au colloids) [16–18]. Compared with the counterparts in SERS, e.g., gold nanocages [17,18], polyhedral silver nanocages were scarcely reported due to the lack of precursor template. Previous works proposed to assemble small nanoparticle building units (typically ~10–50 nm) into mesocrystals or mesostructures by a particle mediated aggregation mechanism [19,20]. The resulting mesosuperstructures are characterized as unique structural features that exhibit rough surface, small size of their building blocks as well as notable internal porosity, making them very appealing as Raman sensor [21–23]. Furthermore, these mesosuperstructures possess typical size of ~ hundreds of nanometers - micrometer, hence create higher-order multipolar plasmonic modes as well as scattering (retardation) effects [24]. As a result, the plasmon resonance band gets noticeably red-shifted and broadened. These effects are important for

* Corresponding author. School of Science, 'Xi'an Jiaotong University, Shann Xi 710049, People's Republic of China.
E-mail address: jxfang@mail.xjtu.edu.cn (J. Fang).

0142-9612/$ – see front matter © 2011 Elsevier Ltd. All rights reserved.
doi:10.1016/j.biomaterials.2011.03.029

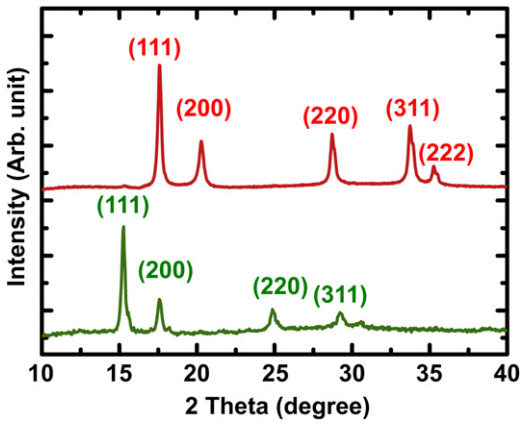

Fig. 1. XRD patterns of Ag_2O octahedrons (green curve) and silver octahedral mesocages (red curve) obtained by the reduction of above Ag_2O octahedrons using H_2O_2 (10%), (Mo radiation). (For interpretation of the references to colour in this figure legend, the reader is referred to the web version of this article.)

applications such as photonics, photocatalysis as well as SERS. In this study, these polyhedral silver mesocages, due to highly rough surface and anisotropic shape effect, 'less-lossy' than gold in the blue/green visible range [25], they show a highly sensitive SERS effect, i.e., $\sim 10^8$–10^9 in magnitude. Importantly, these silver polyhedral mesocages exhibit the highly roughened surface topography due to the fact that the most metals cannot wet the surface of oxide materials [26] and multiple effective hot spots on a single particle (intraparticle effect).

2. Experimental section

2.1. Synthsis of silver polyhedral mesocages

Silver (I) oxide polyhedrons were synthesized by a facile solution-phase route. In a typical synthesis of Ag2O octahedrons, 0.5 M ammonia was added in a dropwise manner into 50 mL 100 mM AgNO3 (aq.) in the presence of various concentrations of poly (vinyl pyrrolidone) (PVP, Mw = 55 000 amu) until the color of the solution turned from tawny to colorless and transparent solution. Then 0.3 mL of 2 M NaOH was rapidly injected into above solution under stirring. Immediately, brownish-black precipitates were obtained. The final products collected by centrifugation and washed several times with distilled water as well as absolute ethanol, subsequently

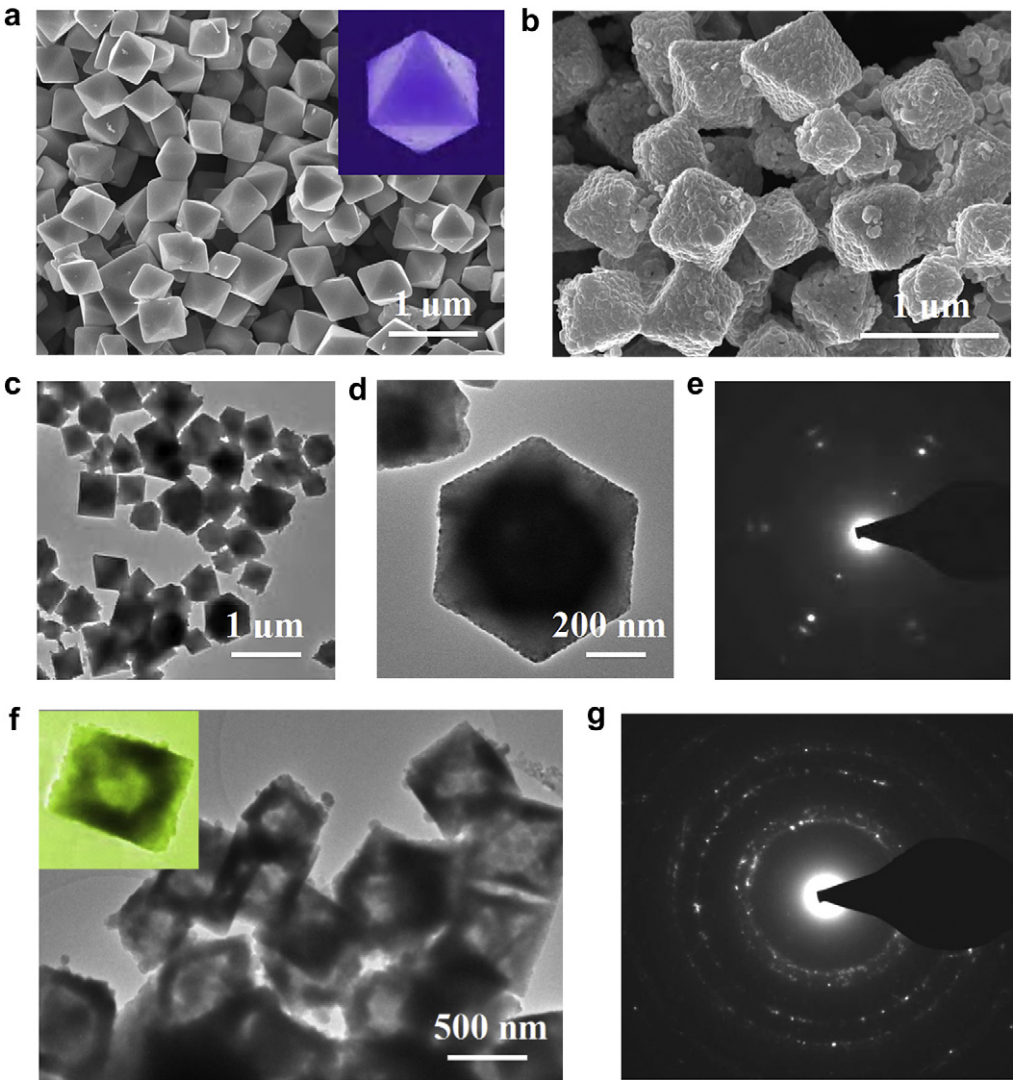

Fig. 2. SEM and TEM images of silver (I) oxide (Ag2O) octahedrons and octahedral Ag mesocages. **a**, SEM and **c, d, e,** TEM images of silver (I) oxide (Ag_2O) octahedrons synthesized at: 100 mM $AgNO_3$ (aq.) 50 mL reacts with 0.5 M ammonia in the presence of 0.1 mM PVP, then reduces by 2 M NaOH. (see text for details). **b**, SEM, **f**, TEM and **g**, SAED pattern of octahedral Ag mesocages obtained by the reduction of above Ag_2O octahedrons using H_2O_2 (10%). The scale bars in Fig. 1a, b, c and Figure f correspond to 1 μm, and 500 nm, respectively.

redispersed in ethanol for further characterization. Other polyhedral Ag2O particles, were synthesized in a similar way except for the concentrations of $AgNO_3$, ammonia and PVP (see details in supplementary information).

In order to synthesize silver mesocages with various polyhedral morphologies, 20 mL of hydrogen peroxide (10%) was added to obtain brownish-black Ag_2O precipitates by dropwise while vigorously magnetic stirring. The solution immediately changed color and evolved gas. The reduced silver mesoparticles were then isolated by centrifugation (2000 rmp, 10 min) and then washed numerous times with water and stored in ethanol for further characterization.

2.2. Characterizations

The general morphology of the products was characterized by LEO 1530 FESEM. The TEM observations were performed with a FEI- Titan 80–300 operated at 300 kV. The TEM samples were prepared by carefully dropping Ag_2O or Ag suspension onto a carbon-coated TEM grid. UV-vis-NIR extinction spectra of Ag mesocanges were measured using Varian Cary 500 spectrophotometer. To evaluate SERS performance, 0.1 mL of the 1×10^{-9} or 1×10^{-11} M aqueous crystal violet (CV) solution were dropped onto the wafer piece (with an area of 10×10 mm^2) coated by synthesized silver mesocages, rinsed with deionized water and dried under ambient conditions. Raman measurements were performed in backscattering geometry with a WiTec CRM200 confocal Raman microscope and a Kaiser Optical RXN1 spectrometer at the excitation wavelengths of 633 nm. The excitation laser spot size and intensity on the samples were typically ~3 μm (i.e. significantly larger than a single mesoparticle size) and 0.1 mW, respectively. Raman imaging of 'hot spots' over mesoparticle arrays was performed on the CRM200 microscope employing a piezo table for sample scanning with a typical X–Y step of 200 nm (200×200 nm^2 scanning pixel size), a high-resolution 100× objective (~ 0.5 μm laser spot) and a spectrum acquisition time of 2 s per pixel. Raman images shown in Fig. 2 represent a color-coded area of the characteristic Raman band of CV at 1172 cm^{-1} integrated over 1120–1250 cm^{-1} with a subtracted broad background signal.

3. Results and discussion

Our general protocol used to synthesize the silver polyhedral mesocages is based on the facile reduction of Ag_2O polyhedrons with hydrogen peroxide (see details in experimental section). Various shapes of the Ag_2O polyhedrons, including sphere, dodecahedron, cube as well as octahedron, serving as the sacrificial templates in this strategy, can be prepared by changing the concentration of the silver ions. Meanwhile, by means of the variation of the concentration of PVP, we can also adjust the sizes for above polyhedral Ag_2O, typically from 300 nm to 1 μm as shown in Figure S1 (Supplementary Information). The chemical compositions of the Ag_2O octahedrons and Ag octahedral mesocages are characterized using X-ray diffraction (XRD) (Fig. 1), giving the signature upon the structural transformation of Ag_2O octahedrons from the cuprite Ag_2O (JCPDS 76-1393) to face-centered cubic Ag (JCPDS 4-783) as the reduction proceeds using the hydrogen peroxide. Fig. 2a shows a typical SEM image of Ag_2O octahedrons with a particle size of around 700 nm. The corresponding TEM images and the SAED pattern shown in Fig. 2c,d and e reveal that the individual Ag_2O octahedral particle is a single crystal. With a reduction process using 10% H_2O_2, the highly surface-roughened Ag octahedrons with uniform octahedral morphology and similar size to that of the Ag_2O template are obtained as demonstrated in Fig. 2b. The TEM image of Ag octahedrons (Fig. 2f and left-up inset) clearly displays the hollow interior. The strong contrast difference between the edges (dark) and center (bright) in Fig. 2f implies that the octahedral mesocages have a wall thickness of around ~ 100 nm. The SAED patterns recorded from single mesocage (shown here for the octahedral, not shown for spherical, dodecahedral and cubic mesocages) reveal the typical polycrystalline nature for all of the obtained polyhedral Ag mesocages. The detailed reduction processes and growth mechanism are investigated by selecting specimens at different reaction times as shown in Scheme 1. Similar to the formation of octahedral Ag mesocages, cubic, dodecahedral as well as spherical Ag mesocages have

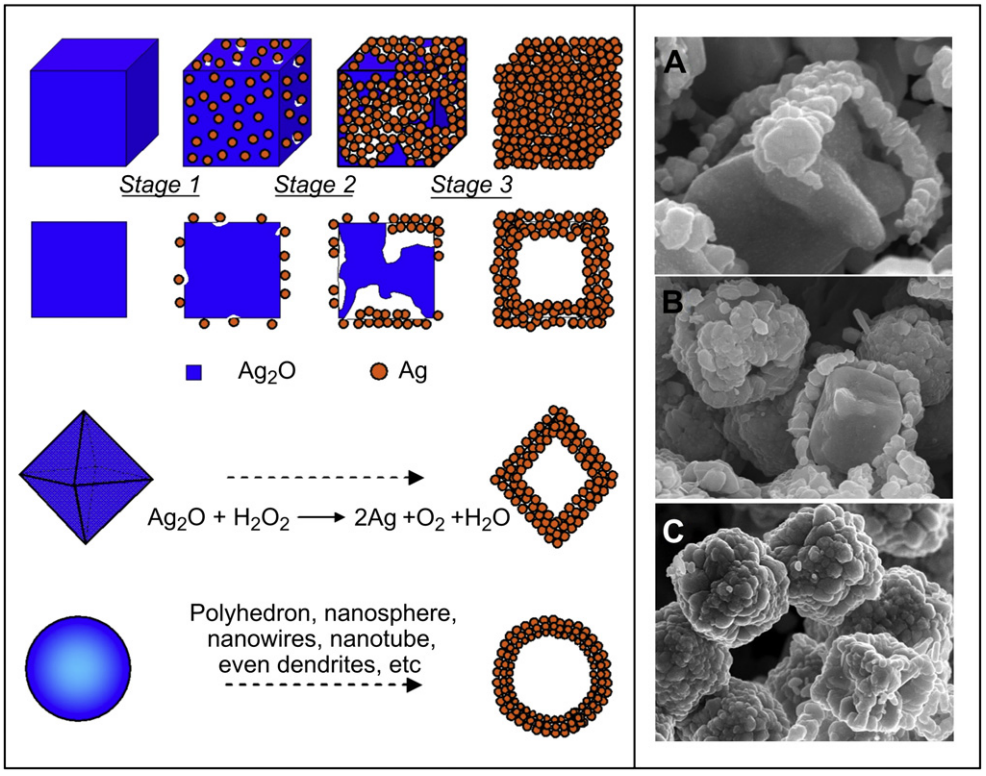

Scheme 1. Schematic illustration summarizing the structural changes involved in the reduction reaction between sacrificial template, e.g., Ag_2O polyhedrons and using H_2O_2 (10%). **Stage 1**: initiation of the reduction reaction at some specific sites; **stage 2**: continuation of the reduction reaction between Ag_2O and H_2O_2 and the formation of a partially hollow nanostructure; and **stage 3**: the formation of "mesoboxes", or other meso-polyhedrons depending on the shape of template. **a, b, c**, show the transition state of cubic Ag mesocages during the reduction process.

also been produced in this study by using various morphological Ag_2O as templates (Fig. 3), respectively.

The investigation of sp-SERS activity for silver polyhedral mesocages was performed by using a confocal Raman microscope with laser excitation at 633 nm. A 1×10^{-9} M crystal violet (CV) aqueous solution, a standard SERS analyte [5,10], was deposited by drop coating onto a Si wafer substrate sparsely coated with the silver mesocage particles. Individual particles on the substrate could be easily observed with an optical microscope. Two types of the Raman experiments were performed. By the first one, the SERS spectra "averaged" over individual particles were acquired by applying a low-magnification objective lens (20 ×). A particle was visually centered within the laser excitation/emission collection spot of ~3 μm. Fig. 4 (left column) shows sp-SERS spectra obtained in this way for individual silver polyhedral mesocages. The highest SERS signals were observed for the octahedral silver mesocages, up to > 10 times higher than the signals from the spherical silver mesocages. The current observations are similar to a recent report on polyhedral silver nanoparticles, where the silver octahedron also manifested the highest SERS effect as compared with silver cube and cuboctahedra [27]. Importantly, in this study, the signals from the octahedral and cubic mesocages were found to be quite reproducible within ±10% from one particle to another (more than 20 particles of each morphology were measured). We may attribute the high SERS reproducibility of silver polyhedral mesocages to their highly roughened surface topography which causes interparticle effect and abundant amount of the effective hot spots in the vicinity of the corrugated and creviced regions between these nanoparticle building units.

By the second type of Raman measurements, SERS signal distributions across individual silver mesocage were characterized (mapped) with a high spatial resolution of ~ 200 nm as provided by a high-magnification objective lens (100×, NA = 0.9) and the confocal mode of the microscope. The mapping was done by moving a substrate with a selected silver particle under the objective with an X–Y piezo table (see Experimental). Fig. 4 (right column) shows typical sp-SERS images of silver polyhedral mesocages. The color code in Fig. 4 represents the intensity of a strong Raman band of CV at 1174 cm^{-1} integrated over 1120–1250 cm^{-1}. Similar to the results of sp-SERS spectra (see above), from comparison of the maximal signals observed (numbers on top of the color-code scale bars), the SERS activity was found to increase in a series: sphere < dodecahedron < cube < octahedron. This observation is consistent with the measurements of the SERS spectra reported above. Moreover, the SERS images of the octahedral and cubic mesocages were found to be quite uniform over their entire surface as illustrated in Fig. 4c–d. Note that the spatial resolution of our

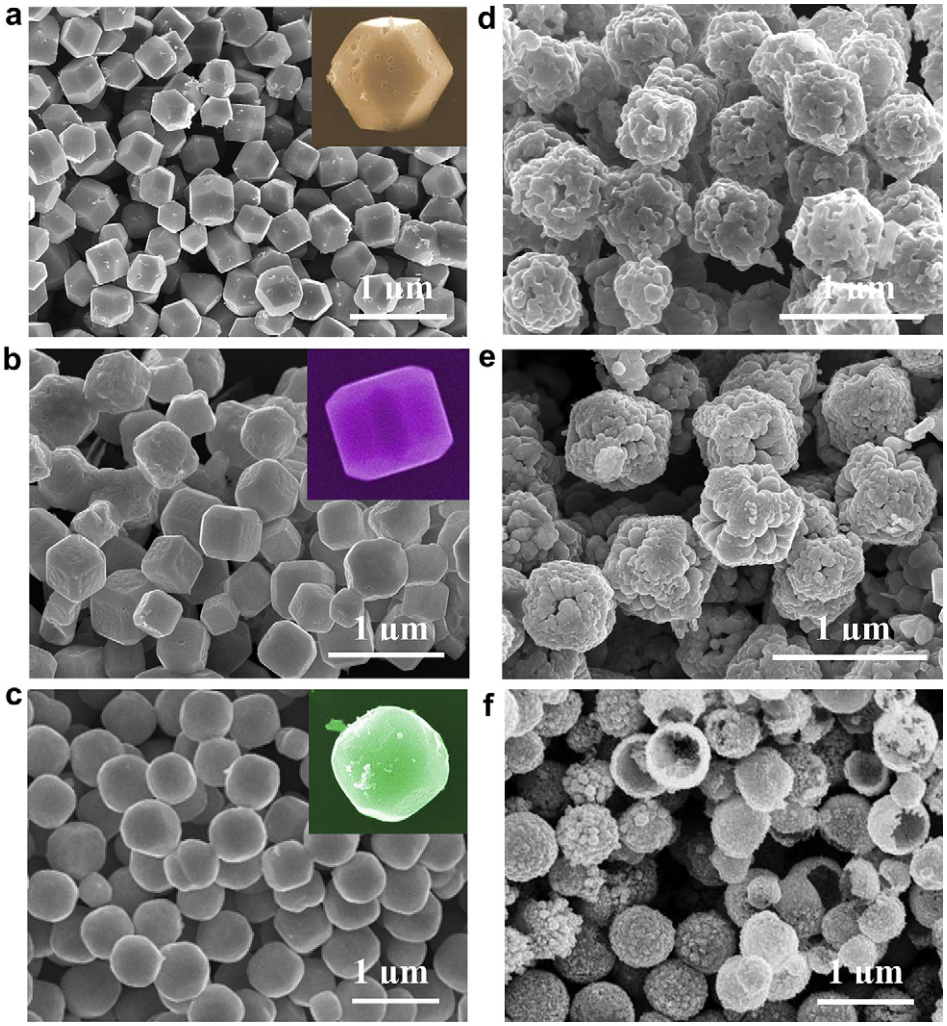

Fig. 3. SEM images of polyhedral silver (I) oxide (Ag2O) and Ag mesocages. Ag_2O polyhedrons synthesized at **a**, dodecahedron, 50 mM $AgNO_3$ (aq.), 0.5 M ammonia, 0.1 mM PVP, 2 M NaOH. **b**, cube, 1 mM $AgNO_3$ (aq.), 0.5 M ammonia, 0.1 mM PVP, 2 M NaOH. **c** sphere, 10 mM $AgNO_3$ (aq.), 0.5 M ammonia, 0.1 mM PVP, 2 M NaOH. **d, e, f**, Ag polyhedral mesocages synthesized by the reduction of above Ag_2O polyhedrons using H_2O_2 (10%).

conventional Raman microscope is by far not sufficient to resolve SERS "hot spots" (on the scale of a few nm). However, the uniform images imply multilple, similarly active "hot spots" homogeneously distributed over the silver octahedral and cubic mesocages – an advantageous feature for sp-SERS sensor.

To corroborate the observed relationship between the SERS activity, structure as well as the surface topography of various silver mesoparticles, we have applied the discrete dipole approximation (DDA) method [28] to calculate the local electric field intensity around model silver particles irradiated with monochromatic light at 514, 633 and 785 nm (Supplementary Information). Four model particles were studied having the same external side length (or diameter) of 400 nm but a different surface texture and structure: (i) smooth cubic shell, (ii) mesocubic shell, (iii) mesocube, and (iv) spherical shell as shown in Fig. 3a–d (not shown for dodecahedral and octahedral mesocages), or, in more detail in Figure S3 (Supplementary Information). The right panels in Fig. 5a–d show typical distributions of the electric field strength E (plotted as color-coded $|E|^2$) calculated in a plane across a vertical axis of these model particles irradiated from above at 633 nm. As one might have anticipated, the most localized and enhanced electric field regions (compare the scale bars in Fig. 5a–d) were found on the whole surface of the highly roughened meso-models. The maximal $|E|^2$ enhancement is found to be about 70, 370, 180 and 130 for models (i)-(iv), respectively. These absolute values do not matter a lot. However, if different models take same conditions of simulation (i.e., grid size, particle size, polarization state, etc), the comparison of these absolute value should be trustable and is sufficient to support the SERS results with different shapes and structures (hollow or solid). In other words, the mesocubic shell structure is clearly favored as the one potentially demonstrating the largest SERS enhancement (proportional to $\sim|E|^4$), in agreement with the experimental results (see above). It is well known that the SERS effect can be optimized when the excitation light wavelength matches to the plasmonic resonance of the metal nanostructure [27]. Our calculations indicate that a dependence of the SERS effect on the excitation wavelength may be especially strong for cubic mesoshell model. This is illustrated by histograms of the maximal electric field ($|E|^2$) enhancement calculated for models (i)-(iv) irradiated at 514, 633 and 785 nm (Fig. 5e). The difference between the models becomes very significant by red-shifting the excitation wavelength to 785 nm, in which the mesocubic shell model shows ~3 times higher field enhancement ($|E|^2$) than that of 514 nm or 633 nm. Compared to the models of smooth or spherical structures, the mesocubic shell has a highly roughened surface texture and anisotropic shape, and therefore likely broadens plasmonic resonances. Taking this into account, our calculations suggest that the optimal SERS excitation wavelength for these particles would lie in the red - near-infrared spectral region. Although the excitation wavelength of larger than 633 nm is not available in our experiment, these may be further supported by UV-vis-NIR spectra which are shown in Figure S4. As the shape of the silver polyhedral mesocages changing to more anisotropic and corners, the localized surface plasmon bands appear in the red and infrared regions of the extinction spectrum.

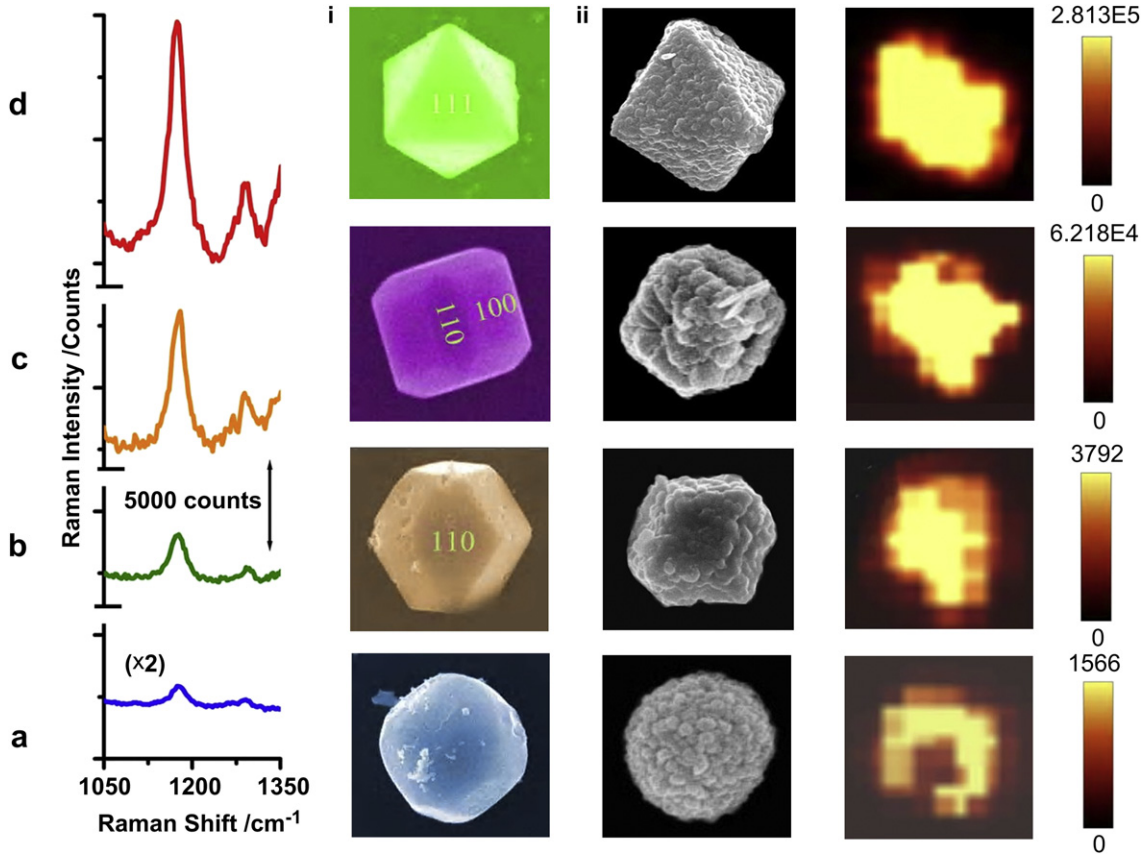

Fig. 4. Single-particle SERS spectra and images of crystal violet (CV) on a polyhedral silver messocages. a, mesospheres, b, mesododecahedron, c, mesocube, d, mesooctahedrons. The color-coded signal of the right column corresponds to the intensity of the Raman band of crystal violet (CV) at 1172 cm^{-1} integrated over 1120–1250 cm^{-1} after background subtraction. The spectra were acquired from individual silver mesostructures on Si substrates under the same conditions (20 s integration time and 0.1 mW excitation power at 633 nm excitation). CV was deposited onto the mesocages on Si substrates by drop coating a 10^{-9} M CV solution. Column i and ii show the typical SEM images of individual polyhedral Ag_2O (i) and Ag (ii) mesostructrues. (For interpretation of the references to colour in this figure legend, the reader is referred to the web version of this article.)

In order to evaluate the sp-SERS performance of the silver polyhedral mesocages at the extreme limit, it is necessary to use a very low number of CV molecules adsorbed. In this study, we deposited CV dye onto the mesocages as described above, but applying a quite diluted solution of CV in water with a concentration of 1×10^{-11} M. According to the estimate in Ref [29] and in the calculation of EFs (Supplementary Information), at this very low CV concentration, a deposition of only a few CV molecules per individual silver particle may be expected. Among these molecules, likely only quite few are adsorbed close enough to different "hot spots" and contribute to the SERS signal. Fig. 6b shows the sp-SERS spectra collected from individual silver cubic mesocages as marked in Fig. 6a (also see the SEM image in Figure S5), under the same conditions as in Fig. 4, but with CV concentration of 1×10^{-11} M. Spectral features close to the characteristic vibrational peaks of CV can be still identified easily. It should be noted that these five particles are randomly chosen, and detectable SERS signals can be acquired in each individual particle. Again, the intensity of SERS signals from such random particles indicates a good repeatability even at the very low coverage with CV analyte molecules (except for particle-v which is the particle/particle aggregate). In this regard, the high activity and reproducibility of polyhedral silver mesocages make them suitable for highly sensitive sp-SERS substrates. Previous investigations on angular dependence of SERS activities indicate that the laser polarization needs to be taken into account whenever supported, nonspherical nanoparticles are involved. Therefore, in this study, to understand the dependence of SERS signal on laser polarization, we conducted the DDA calculation for the mesocubic shell model (ii). Fig. 6c shows the E-field amplitude patterns for the model of mesocubic shell (ii) that is irradiated with light polarized in the 0°, 15°, 30°, and 45°deviated from *x*-axis. The incident polarization angle dependent maximum field enhancement (Fig. 6d) demonstrates that the E-field intensity difference of various polarization angles is less than ±6%. This value would not show much polarization dependency. Furthermore, experimentally, nearly all the random selected mesoparticles, which include the polarized effect, can show the robust and reproducible sp-SERS signals even at the current quite low coverage of CV molecules (1×10^{-11} M).

A SERS enhancement factor (EF) is a quantitative measure of the Raman signal amplification for a specific analyte. Following the procedure reported by Wang et al. [30] and employing the CV peak

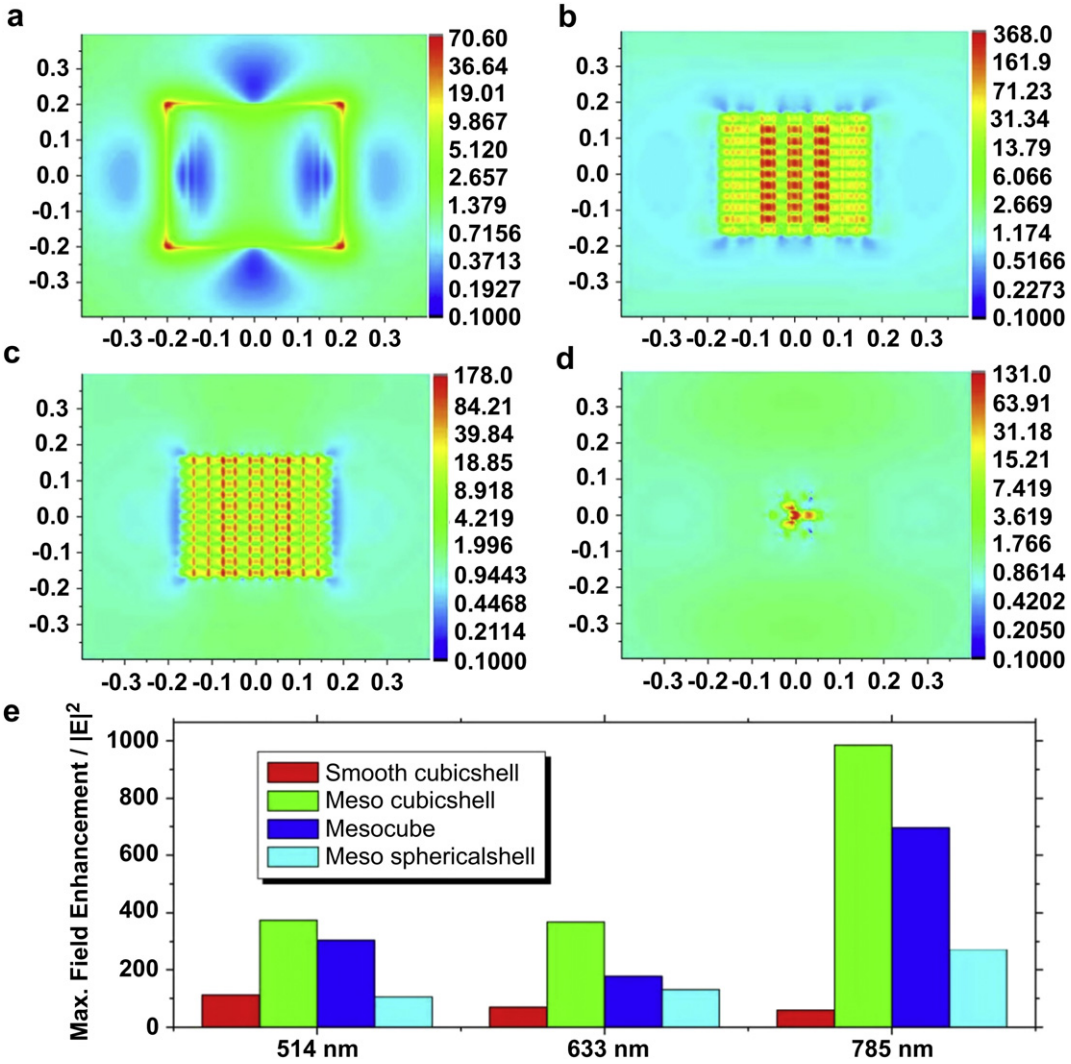

Fig. 5. E-field amplitude patterns of individual particles. Model silver particles with same external side length (or diameter) of 400 nm and corresponding calculated distributions of the local electric field intensity (color-coded relative $|E|^2$ values) across air-suspended particles irradiated from top at 633 nm. **a**, smooth cubic shell with inner side length of 300 nm, **b**, mesocubic shell with inner side length of 300 nm, **c**, mesocube, and **d**, spherical shell with inner diameter of 300 nm. **e**, maximal electric field enhancements calculated for models (i-iv) at the excitation wavelengths of 514, 633 and 785 nm, respectively.

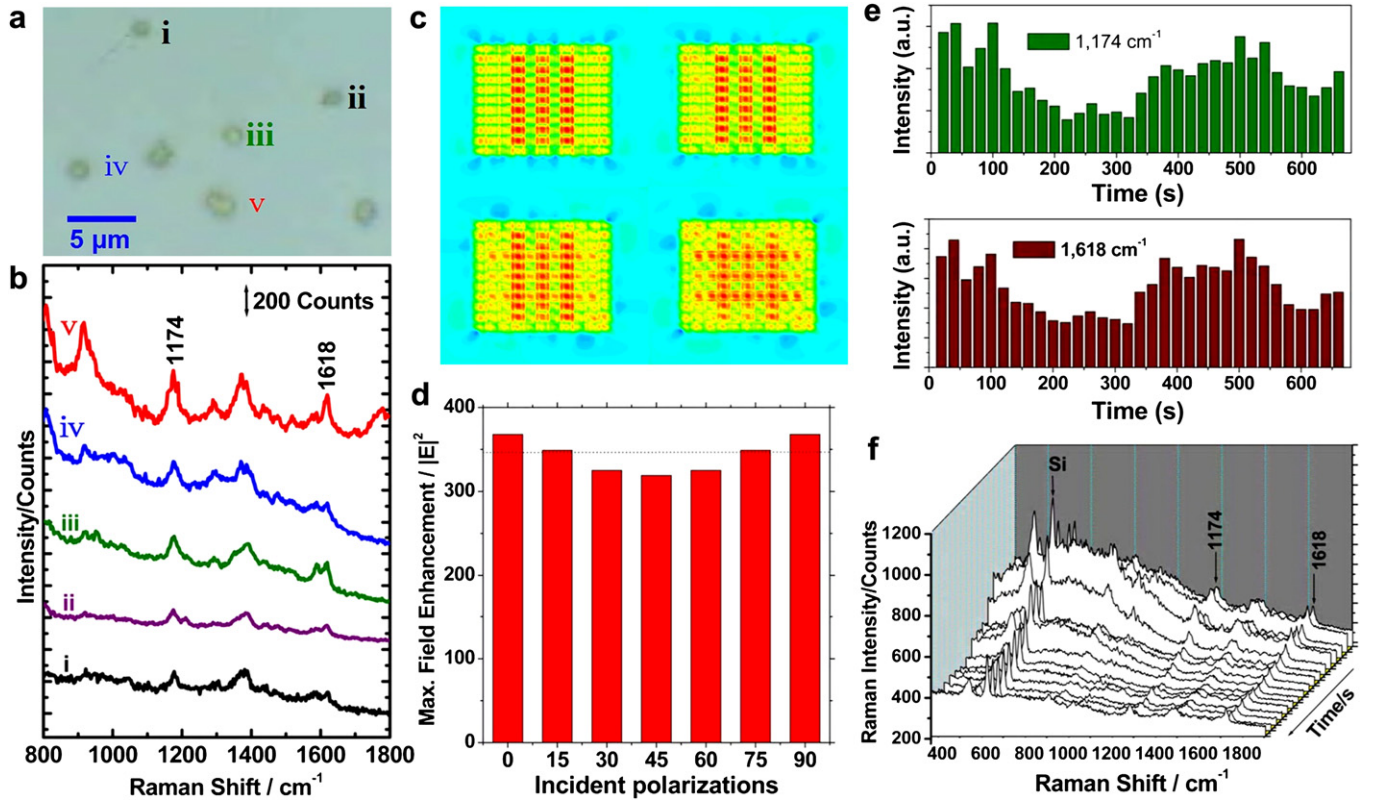

Fig. 6. Single-molecule behaviors from individual silver cubic mesocage. **a,** Optical microscopy, and, **b,** corresponding sp-SERS spectra with CV analyte molecules (1×10^{-11} M). **c,** the E-field amplitude patterns of the model of mesocubic shell (ii) for different incident polarizations. **d**, the incident polarization angle dependent maximum field enhancement, **e**, Peak heights of the 1174 cm^{-1} line and 1618 cm^{-1} line for the SERS spectra scanning > 10 min (all spectra were measured with the same collection time, 20 s, and incident laser power, 0.1 mW). **f**, time-resolved blinking sp-SERS spectra taken from the silver cubic mesocage.

at 1174 cm^{-1} as shown in Fig. 4 (the strongest peak in the spectra), we estimated EFs to be about $\sim 10^8$–10^9 for the individual octahedral and cubic silver mesocages, respectively (See supplementary information). Taking into account the roughened surface of the mesocages, the above mesocage area may be underestimated and the EFs, consequently, overestimated. On the other hand, rinsing the substrates after CV deposition with water (see Experimental) can remove a significant fraction of CV molecules (assuming 1%~10% residual in Ref [30]) and thus the EFs, in this study, may be underestimated. It should be noted that our estimate of EFs seems reasonable, corresponding to that reported by Liang (EF $\sim 10^7$–10^8) for "flower-like" silver nanoparticles [19] which show quite a similar surface morphology and size as our spherical mesocages. Meanwhile, in this study, combining the anisotropic effect and hollow interior (see above in Figs. 4 and 5), 1–2 orders of magnitude higher EFs have been achieved for individual silver octahedral and cubic mesocages, respectively, compared with spherical shell in this study (Fig. 4) and the "flower-like" silver nanoparticles in Ref. [19]. Also note that the EFs obtained here are the average values over a mesoparticle surface due to a relatively large laser excitation spot (~3 μm) on the samples. Correspondingly, EF at 'hot spots' may significantly exceed the above values (probably $>10^9$ or 10^{10}, or even higher) on some special sites where the effective hot spots are highly localized, if measured with a higher spatial resolution. Furthermore, we would like to emphasize that the above estimates are for the single particles only. However, even higher EFs may also be expected for aggregates or close-packed arrays of the mesocages: such SERS substrates are usually more active (typically 1–2 magnitudes higher) than the particles forming them, because of the interparticle interactions generating additional "hot spots" (for instance, in tiny gaps between the neighbor nanoparticles) [18,19]. Thus, the aggregates or arrays made by the obtained octahedral or cubic silver mesocages could be reasonable to show an EF of $\sim 10^9$–10^{10} according to the interparticle effect [18,19].

Further evidence for the highly sensitive SERS behavior was made by applying time-resolved sp-SERS spectra recorded at 20 s intervals as shown in Fig. 6e–f. The sp-SERS spectra in the "few CV molecules regime" demonstrated strong temporary fluctuations in the intensity (Fig. 6e) and frequency position (Fig. 6f) of vibrational features. A time-dependent reversible on/off "blinking" phenomenon was clearly observed which indicates the presence of a single molecule. The "blinking effect" has been discussed as a hallmark of a single molecule-SERS detection and attributed to the thermally and non-thermally activated diffusion of molecules as well as to their transformations, e.g., via (de) protonation [29,31]. Although "blinking" phenomena are apparently disadvantageous for analytical applications, the observed sp-SERS response evidences a remarkably high SERS activity of silver octahedral and cubic mesocages. We also note the question that is related to the minimum EF needed to see single molecule-SERS. According to recent investigations [26,32,33], it seems that EFs in the order of $\sim 10^{10}$–10^{11} can actually be used to see single molecules which have differential cross sections in the typical range of $\sim 10^{-29}$–10^{-30} cm^2/sr for nonresonant molecules, and $\sim 10^8$ are even enough to see resonant single molecules with differential cross sections $\sim 10^{-27}$ cm^2/sr. In this regard, some special sites on the highly roughened surface or the aggregates of the polyhedral silver mesostructures may approach a single molecule-SERS detection limit.

4. Conclusions

In summary, via a mesotransformation protocol, we synthesize a silver mesosuperstructure –polyhedral mesocages, particularly the octahedral and cubic silver mesocages, which display high sensitivity with high structural reproducibility. These results are significant for the following reasons. First, the mesotransformation protocol is a suitable route to assemble nanoparticle building units into desired nanostructure or mesosuperstructure by means of various growth mechanisms, which allow us to explore hot SERS structure in an efficient and straightforward fashion. Second, owing to the unique structural features of mesosuperstructure-highly roughened-surface topography combining abundant amount of corrugated, creviced regions between these nanoparticle building units as well as the anisotropic effect, the resulting single mesoparticle may exhibit a high SERS sensitivity. Third, the intraparticle interaction between the nanoparticle building units within the single mesoparticle create multiple homogenously-distributed effective hot spots, herein, increases the reproducibility and reliability for the sp-SERS. Fourth, the obtained EF is an "average" value, i.e., $\sim 10^8-10^9$ magnitude, and some special sites where the effective hot spots concentrate could show a higher EFs, e.g., $> 10^{10}$, approaching the single molecule-SERS limit. That may be one of the reasons why the silver cubic mesocages obtained in this study may show detectable 'single molecule-like' sp-SERS signals. Fifth, the SERS activity would be further improved by the aggregation or close-packed arrays of the result octahedral or cubic mesocages because of interparticle interactions generating additional "hot spots". Finally, compared with lithographically produced SERS substrates, the current protocol combines the high performance (quite unusual EFs and considerable reproducibility), simple processes as well as low cost. As such, the current protocol opens avenues for the fabrication of structurally reproducible mesosuperstructure-based SERS sensors.

Acknowledgment

We thank Prof, B. J. Ding, in 'Xi'an Jiaotong University, China, and Drs. Frank Schramm and Di Wang at Karlsruhe Institute of Technology (KIT), Institute of Nanotechnology, Germany, for the helpful discussions. J. X. Fang is grateful to Alexander-von-Humboldt Foundation for the fellowship to support his researches in Germany. J. X. Fang was supported by the Tengfei Talent project of 'Xi'an Jiaotong University, "the Fundamental Research Funds for the Central Universities (No. 08142008), and "the National Natural Science Foundation of China (Nos. 50901056, 5107116)". Z. Y. Li was supported by the National Natural Science Foundation of China under Grant Nos. 60736041 and 10874238.

Appendix. Supplementary data

Supplementary data associated with this article can be found, in the online version, at doi:10.1016/j.biomaterials.2011.03.029.

References

[1] Li JF, Huang YF, Ding Y, Yang ZL, Li SB, Zhou XS, et al. Shell-isolated nanoparticle-enhanced Raman spectroscopy. Nature 2010;464:392–5.
[2] Smythe EJ, Dickey MD, Bao JM, Whitesides GM, Capasso F. Optical antenna arrays on a fiber facet for in situ surface-enhanced Raman scattering detection. Nano Lett 2009;9:1132–8.
[3] Fofang NT, Park TH, Neumann O, Mirin NA, Nordlander P, Halas NJ. Plexcitonic nanoparticles: plasmon-exciton coupling in nanoshell-J-aggregate complexes. Nano Lett 2008;8:3481–7.
[4] Nie S, Emory SR. Probing single molecules and single nanoparticles by surface-enhanced Raman scattering. Science 1997;275:1102–6.
[5] Kneipp K, Wang Y, Kneipp H, Perelman LT, Itzkan I, Dasari RR, et al. Single molecule detection using surface-enhanced Raman scattering (SERS). Phys Rev Lett 1997;78:1667–70.
[6] Zhang XY, Hicks EM, Zhao J, Schatz GC, Van Duyne RP. Electrochemical tuning of silver nanoparticles fabricated by nanosphere lithography. Nano Lett 2005;5:1503–7.
[7] Li W, Camargo PHC, Lu X, Xia YN. Dimers of silver nanospheres: facile synthesis and their use as hot spots for surface-enhanced Raman scattering. Nano Lett 2009;9:485–90.
[8] Li ZY, Xia YN. Metal nanoparticles with gain towards single-molecule detection by surface-enhanced Raman scattering. Nano Lett 2010;10:243–9.
[9] Gopinath A, Boriskina SV, Premasiri WR, Ziegler L, Reinhard BM, Negro LD. Plasmonic nanogalaxies: multiscale aperiodic arrays for surface-enhanced Raman sensing. Nano Lett 2009;9:3922–9.
[10] Qian X-M, Nie SM. Single-molecule and single-nanoparticle SERS: from fundamental mechanisms to biomedical applications. Chem Soc Rev 2008;37:912–20.
[11] Rodríguez-Lorenzo L, Alvarez-puebla RA, Pastoriza-Santos I, Mazzucco S, Stephan O, Kociak M, et al. Zeptomol detection through controlled ultrasensitive surface-enhanced Raman scattering. J Am Chem Soc 2009;131:4616–8.
[12] Pettinger B, Ren B, Picardi G, Schuster R, Ertl G. Nanoscale probing of adsorbed species by tip-enhanced Raman spectroscopy. Phys Rev Lett 2004;92:096101–4.
[13] Nelayah J, Kociak M, Stephan O, Abajo FJG, Tence M, Henrard L, et al. Mapping surface plasmons on a single metallic nanoparticle. Nat Phys 2007;3:348–53.
[14] Fang Y, Seong NH, Dlott DD. Measurement of the distribution of site enhancements in surface-enhanced Raman scattering. Science 2008;321:388–92.
[15] Lim DK, Jeon KS, Kim HM, Nam JM, Suh YD. Nanogap-engineerable Raman-active nanodumbbells for single-molecule detection. Nat Mater 2010;9:60–7.
[16] Yavuz MS, Cheng YY, Chen JY, Cobley CM, Zhang Q, Rycenga M, et al. Gold nanocages covered by smart polymers for controlled release with near-infrared light. Nat Mater 2009;8:935–9.
[17] Rycenga M, Wang ZP, Gordon E, Cobley CM, Schwartz AG, Lo CS, et al. Probing the photothermal effect of Au-based nanocages with surface-enhanced Raman scattering. Angew Chem Int Ed 2009;48:9924–7.
[18] Ei-Sayed MA, Mahmoud MA. Aggregation of gold nanoframes reduces, rather than enhances, SERS efficiency due to the trade-off of the inter-and intra-particle plasmonic fields. Nano Lett 2009;9:3025–30.
[19] Fang JX, Leufke PM, Kruk R, Wang D, Scherer T, Hahn H. External electric field driven 3D ordering architecture of silver (I) oxide meso-superstructures. Nanotoday 2010;5:175–80.
[20] Niederberger M, Cölfen H. Oriented attachment and mesocrystals: non-classical crystallization mechanisms based on nanoparticle assembly. Phys Chem Chem Phys 2006;8:3271–87.
[21] Wang H, Halas NJ. Mesoscopic Au "meatball" particles. Adv Mater 2008;20:820–5.
[22] Liang HY, Li ZP, Wang WZ, Wu YS. Xu, H X. Highly surface-roughened "flower-like" silver nanoparticles for extremely sensitive substrate of surface-enhanced Raman scattering. Adv Mater 2009;21:4614–8.
[23] Fang JX, Du SY, Li ZY, Lebedkin S, Kruk R, Hahn H. Gold mesocrystals with tailored surface topography and self-assembly arrays for surface enhanced Raman spectroscopy. Nano Lett 2010;10:5006–13.
[24] Kumbhar AS, Kinnan MK, Chumanov G. Multipole plasmon resonances of submicron silver particles. J Am Chem Soc 2005;127:12444–5.
[25] Etchegoin PG, Le Ru EC. A perspective on single molecule SERS: current status and future challenges. Phys Chem Chem Phys 2008;10:6079–89.
[26] Hu M, Chen JY, Li ZY, Au L, Hartland GV, Li XD, et al. Gold nanostructures: engineering their plasmonic properties for biomedical applications. Chem Soc Rev 2006;35:1084.
[27] Mulvihill M, Ling XY, Henzie J, Yang PD. Anisotropic etching of silver nanoparticles for plasmonic structures capable of single-particle SERS. J Am Chem Soc 2010;132:268–74.
[28] Yurkin MA, Hoekstra AGJ. The discrete dipole approximation: an overview and recent developments. J Quantitative Spectr Radiative Transfer 2007;106:558–89.
[29] Xu HX, Bjerneld EJ, Kall M. Borjesson, L. Spectroscopy of single Hemoglobin molecules by surface enhanced Raman scattering. Phys Rev Lett 1999;83:4357–62.
[30] Wang Y, Becker M, Wang L, Liu JQ, Scholz R, Peng J, et al. Nanostructured gold films for SERS by block copolymer-templated galvanic displacement reactions. Nano Lett 2009;9:2384–9.
[31] Jiang J, Bosnick K, Maillard M, Brus L. Single molecule Raman spectroscopy at the junctions of large Ag nanocrystals. J Phys Chem B 2003;107:9964–9.
[32] Shim S, Stuart CM, Mathies RA. Resonance Raman Cross-Sections and Vibronic Analysis Of Rhodamine 6G from Broadband Stimulated Raman spectroscopy. ChemPhysChem 2008;9:697–702.
[33] Blackie EJ, Ru ECL, Etchegoin PG. Single-molecule surface-enhanced Raman spectroscopy of nonresonant molecules. J Am Chem Soc 2009;131:14466–72.